Received: 14 August 2019 | Revised: 15 November 2019 | Accepted: 15 November 2019

DOI: 10.1002/jrs.5805

RESEARCH ARTICLE

Journal of RAMAN SPECTROSCOPY WILEY

Shift in the Raman symmetric stretching band of N_2, CO_2, and CH_4 as a function of temperature, pressure, and density

D. Matthew Sublett Jr.[1] | **Eszter Sendula**[1] | **Hector Lamadrid**[2] | **Matthew Steele-MacInnis**[3] | **Georg Spiekermann**[4] | **Robert C. Burruss**[5] | **Robert J. Bodnar**[1]

[1]Department of Geosciences, Virginia Tech, Blacksburg, Virginia, USA

[2]Department of Geological Sciences, University of Missouri, Columbia, Missouri, USA

[3]Department of Earth & Atmospheric Sciences, University of Alberta, Edmonton, Alberta, Canada

[4]Institut für Geowissenschaften, Universität Potsdam, Potsdam, Germany

[5]United States Geological Survey, Reston, Virginia, USA

Correspondence
D. Matthew Sublett Jr., Department of Geosciences, Virginia Tech, 4044 Derring Hall, 926 West Campus Drive, Blacksburg 24061, VA.
Email: dsublett@vt.edu

Funding information
National Science Foundation, Grant/Award Numbers: EAR-1624589, OCE-1459433

Abstract

The Raman spectra of pure N_2, CO_2, and CH_4 were analyzed over the range 10 to 500 bars and from −160°C to 200°C (N_2), 22°C to 350°C (CO_2), and −100°C to 450°C (CH_4). At constant temperature, Raman peak position, including the more intense CO_2 peak ($\nu+$), decreases (shifts to lower wave number) with increasing pressure for all three gases over the entire pressure and temperature (*PT*) range studied. At constant pressure, the peak position for CO_2 and CH_4 increases (shifts to higher wave number) with increasing temperature over the entire *PT* range studied. In contrast, N_2 first shows an increase in peak position with increasing temperature at constant pressure, followed by a decrease in peak position with increasing temperature. The inflection temperature at which the trend reverses for N_2 is located between 0°C and 50°C at pressures above ~50 bars and is pressure dependent. Below ~50 bars, the inflection temperature was observed as low as −120°C. The shifts in Raman peak positions with *PT* are related to relative density changes, which reflect changes in intermolecular attraction and repulsion. A conceptual model relating the Raman spectral properties of N_2, CO_2, and CH_4 to relative density (volume) changes and attractive and repulsive forces is presented here. Additionally, reduced temperature-dependent densimeters and barometers are presented for each pure component over the respective *PT* ranges. The Raman spectral behavior of the pure gases as a function of temperature and pressure is assessed to provide a framework for understanding the behavior of each component in multicomponent N_2-CO_2-CH_4 gas systems in a future study.

KEYWORDS

fluids, wave number, attraction, repulsion

1 | INTRODUCTION

Natural fluids in which N_2, CO_2, and CH_4 are major constituents are common in metamorphic environments,[1–5] sedimentary basins,[6,7] and in some ore-forming environments.[8,9] They have also been identified in the atmosphere and at the surface of some celestial bodies such as Titan, an icy moon of Saturn.[10,11] Furthermore, gas mixtures with similar compositions are commonly part of industrial processes, as well as in agricultural and

municipal waste management, for example, in the production of biofuels that are increasingly used for generating heat and electricity.[12,13] Thus, methods to analyze the physical and chemical properties of these gases and gas mixtures are needed for a variety of applications.

Raman spectroscopy offers a nondestructive method to characterize the properties of a wide variety of natural and synthetic materials. The intensity, width, and wave number (hereafter, referred to as "peak position") of a Raman peak provide information on the bonding environment of the molecules in the material of interest.[14] Raman peak positions of fluids have been shown to vary as functions of pressure, temperature, and density.[4,15–37] Shifts in the Raman peak position of fluids with changing conditions have been related to the attractive and repulsive forces between molecules: attractive forces cause Raman peak position to shift to lower wave number, whereas repulsive forces cause Raman peak position to shift to higher wave number, and the overall direction of peak shift with changing conditions implies dominance of either attractive or repulsive forces.[21,27,38–40]

The N_2 molecule has only one fundamental vibrational mode, the symmetric stretching of the N≡N bond, which is Raman active at approximately 2,330 cm^{-1} at 1 bar.[41] Several studies have investigated the change in the Raman spectral properties of N_2 over a range of pressures at room temperature,[19,23,24] at low temperatures near or below the critical point,[25,27] at elevated temperatures,[28,30,42] and in gas mixtures.[13,15,19,31]

The CH_4 molecule exhibits four fundamental vibrational modes that are Raman active, at approximately 3,019, 2,917, 1,534, and 1,309 cm^{-1} at 1 bar, but only the 2,917-cm^{-1} mode (ν_1), which represents the symmetric stretching of the C—H bond, is commonly observed in Raman spectra.[4] The shift in Raman peak position of the symmetric stretching mode of CH_4 with pressure has been studied at room temperature,[16,17,22,32–34] at lower temperatures down to −150°C,[16,17,34] at elevated temperatures,[34] and in mixtures.[13,15,19,31,35–37]

Due to its linear geometry, CO_2 should show only one fundamental vibrational mode that is Raman active (symmetric stretching of the C?O bond) at approximately 1,333 cm^{-1}. However, this mode exhibits nearly the same energy as the first overtone of the infrared-active bending mode.[43] The interaction between these two modes results in a splitting of the 1,333 cm^{-1} vibrational band into two bands, nominally located at 1,388 and 1,285 cm^{-1} at 1 bar, in a process known as Fermi resonance.[4,44] These two peaks are referred to as the Fermi diad, and the distance between the two peaks has been used to estimate the density of CO_2.[18–20,44–47]

In this study, we explore the vibrational properties of pure N_2, CH_4, and CO_2 over broad pressure and temperature (*PT*) ranges to investigate the relationships between Raman spectral features, pressure, and temperature. We interpret the results in terms of relative volumetric (density) changes, attractive and repulsive forces between molecules, and proximity to the critical point. This study thus expands the available Raman peak shift data on N_2, CH_4, and CO_2 to a larger *PT* range and provides a starting point for examining variations in Raman spectral properties of these gases in higher order systems in future studies.

2 | METHODS

Raman spectra for N_2, CH_4, and CO_2 were collected from 10 to 500 bars over temperature ranges of −160°C to 200°C (N_2), −100°C to 450°C (CH_4), and 22°C to 350°C (CO_2) using a JY Horiba LabRam HR (800-mm spectrometer) Raman microprobe equipped with a high-pressure optical capillary system (similar to that described by Chou et al.[48]) and a Linkam CAP500 capillary heating and cooling stage. The Raman microprobe is equipped with an 1,800-grooves per millimeter grating, a slit width of 150 μm, a confocal aperture of 400 μm, and a 40× microscope objective (numerical aperture = 0.55). Excitation was provided by a 514-nm Laser Physics 100S-514 Ar^+ laser with an output power at the source of 50 mW. The lower temperature limit at which data were obtained for each gas corresponds to the intersection of the liquid–vapor (L–V) curve for that gas along the isobar of interest, whereas the higher temperature limits reflect the decrease in signal strength with increasing temperature that precluded determination of Raman peak positions. The lower pressure limit is defined by the lowest pressure at which peaks with sufficient intensity above background to be quantified could be recorded, and the upper pressure limit was arbitrarily chosen to be 500 bars. Gases were commercially prepared by Airgas, Inc (99.999% pure).

The Linkam CAP500 capillary heating and cooling stage was connected to two manual pressure generators (HiP Model 37-6-30) that allow the pressure inside the capillary tube to be controlled and varied. Generally, measurements along an isotherm began at low pressure, with the piston positioned such that it is mostly retracted from the sample cell, thus maximizing the sample volume. Starting at 10 bars, the pressure is increased incrementally, and the Raman peak position for the gas of interest was determined at each pressure along the isotherm until the maximum pressure (500 bars) was reached. Then the temperature was changed, and the process was repeated along that new isotherm. Additional details of the pressure system have been

published elsewhere.[16–20] Pressure was monitored using a precise instruments pressure transducer (Model 645). The error in the pressure measurements was ±0.1% of the total output pressure reading. Temperature was monitored using the internal thermocouple of the CAP500 stage with an error in the temperature measurements of no more than ±0.4% of the total output temperature reading.

Raman analyses were conducted through a transparent 20-cm long square flexible fused silica capillary tube with an outer diameter of ~363 μm and an inner diameter of ~100 μm, prepared by Polymicro Technologies, LLC. Raman measurements were collected from the center of a 5-cm long portion of the capillary that was heated/cooled within the stage. The thermal gradient along this 5-cm portion is reported by Linkam to be ±0.2% of the total output temperature at the edges relative to the center. Spectra were collected only after the temperature and pressure stabilized and remained constant, with equilibration periods of at least 1 min after the pressure was changed and 10 min following a change in temperature. Collection times were selected to ensure that the Raman peaks of interest consisted of at least four data points above the background noise, with CO_2 and N_2 requiring the longest collection times (~180 s at 10 bars) and CH_4 requiring the shortest (~40 s at 10 bars). The collection times required to satisfy our threshold of at least four points above background noise decreased with increasing pressure and decreasing temperature. Certain low-pressure, high-temperature conditions were excluded from this study because spectra at these conditions, especially for N_2 and CO_2, did not show at least four data points above background noise. Additionally, the peak intensity to full width at half maximum (FWHM) ratio for each peak was never less than 500 counts/cm^{-1} and in most cases was greater than 1,000 counts/cm^{-1}. Both selection criteria, the peak intensity to FWHM ratio and at least four data points above the noise, are applied to all peaks collected in this study, including both the more and less intense peaks that make up the Fermi diad. Three accumulations were collected for each gas, and this was repeated three times at each *PT* condition to produce three data points at each *PT* point and to assess the precision in the measurements. The average variation in the Raman peak positions of N_2, CO_2, and CH_4 was ±0.01, ±0.02, and ± 0.01 cm^{-1}, respectively, and the average variation in the Fermi diad measurements was ±0.02 cm^{-1}. The Raman peak positions calculated from each of the three collections were averaged and used in all subsequent data analyses discussed below.

The peaks recorded in this study include the symmetric stretching modes of N_2 (N≡N) and CH_4 (C—H), nominally located at 2,331 and 2,917 cm^{-1} at 1 bar, respectively; and the two peaks that comprise the Fermi diad of CO_2, nominally located at 1,388 and 1285 cm^{-1} at 1 bar. Ne lines bounding the peaks of interest (N_2, 2,253.58 and 2,433.93 cm^{-1}; CO_2, 1,031.42 and 1,458.58 cm^{-1}; and CH_4, 2,851.49 and 2,972.55 cm^{-1}) were collected simultaneously with each gas analysis to correct for spectrometer drift, following the correction method of Lin et al.[17]

$$\nu^{i}_{\mathrm{corr}} = \frac{1}{2}\left\{\left[\nu^{i}_{\mathrm{measured}} + \left(\nu^{\mathrm{Ne},-}_{\mathrm{real}} - \nu^{\mathrm{Ne},-}_{\mathrm{measured}}\right)\right] + \left[\nu^{i}_{\mathrm{measured}} + \left(\nu^{\mathrm{Ne},+}_{\mathrm{real}} - \nu^{\mathrm{Ne},+}_{\mathrm{measured}}\right)\right]\right\}, \quad (1)$$

where Ne± are the Ne emission lines that occur at higher (+) and lower (−) wave numbers compared with the peak for the gas, real is the known position of the Ne emission line, and measured is the measured position of the Ne emission line. All spectra were fit using LabSpec 5 software first using a linear baseline correction and then a Gaussian–Lorentzian peak fitting function.

Several recent studies have shown that although the absolute peak position at a given *PT* condition shows slight variation from one study to another owing to laboratory and instrument specific factors, all studies show similar parallel trends in the variation in peak position with pressure.[20,35] As such, to allow comparison between our new data and other published data, our results at 22°C were corrected to be consistent with data from Fall et al.[18] for CO_2 and Lin et al.[16] for CH_4. These studies chosen for inclusion were selected because they were conducted using the same Raman microprobe, and the same data collection and analysis procedure, that was used in this study. That is, if at 22°C and some pressure our measured peak position was, for example, 0.04 cm^{-1} higher than that reported in the studies referred to above for the same gas at the same *PT* condition, we systematically subtracted 0.04 cm^{-1} from our determined peak position to bring the results from the two studies into agreement. We also note, as has been

described by Lamdarid et al.[20] and Lu, Chou, Burruss, and Song,[35] that the magnitude of the difference varied slightly from day to day; as such, the correction factor was determined before each analytical session and applied to the data collected during that session. Because there were no data for N_2 at 22°C in the literature that were collected using the same Raman system and collection protocol as used here, we determined our own calibration curve at this temperature and then used these results to correct the N_2 peak positions in all subsequent analyses. The only Raman spectral feature of interest in this study was peak position; accordingly, the FWHM, peak areas, and intensities of the peaks are not reported here. However, Figure S1 shows the relative change in peak intensity and width under changing *PT* conditions for each gas. All Raman peak positions and Fermi diad splitting measurements collected in this study, as well as the error in the Raman measurements determined, calculated densities, and compressibility factors, are presented in Appendix A.

3 | RESULTS

3.1 | Isothermal peak shift with changing pressure

The relationship between pressure and Raman peak position over the temperature range of interest for each species is shown in Figure 1. The critical point for CH_4 (Figure 1a) is located at −83°C and 46 bars. For all isotherms that are above the critical temperature (−83°C), the L–V curve is not intersected as the pressure is increased and there is a smooth and continuous variation in peak position as a function of pressure. However, the L–V curve is intersected at ~23 bars along the −100°C isotherm. That is, during the experiment, as the pressure was increased from 10 bars at −100°C, the L–V curve for CH_4 is intersected at ~23 bars and liquid begins to condense from the vapor. At this point, the pressure remains constant until all of the vapor phase has condensed into liquid as the sample cell volume is decreased. This phase transition leads to a discontinuity in peak position versus pressure along the −100°C isotherm in Figure 1a represented by the dashed portion of the isotherm. At this condition, if one were to focus the laser in the vapor phase, a peak position corresponding to the density of the vapor phase on the L–V curve would be obtained; similarly, if the laser were focused on the liquid phase, a peak position corresponding to the density of the liquid phase on the L–V curve would be obtained.

For CH_4, the peak position decreases with increasing pressure at constant temperature over the entire temperature range studied (Figure 1a), and the CH_4 peak position increases with increasing temperature at constant pressure over the entire pressure range studied. Also shown on Figure 1a is the critical point and the projection of the critical isochore for CH_4. Note that conditions to the left

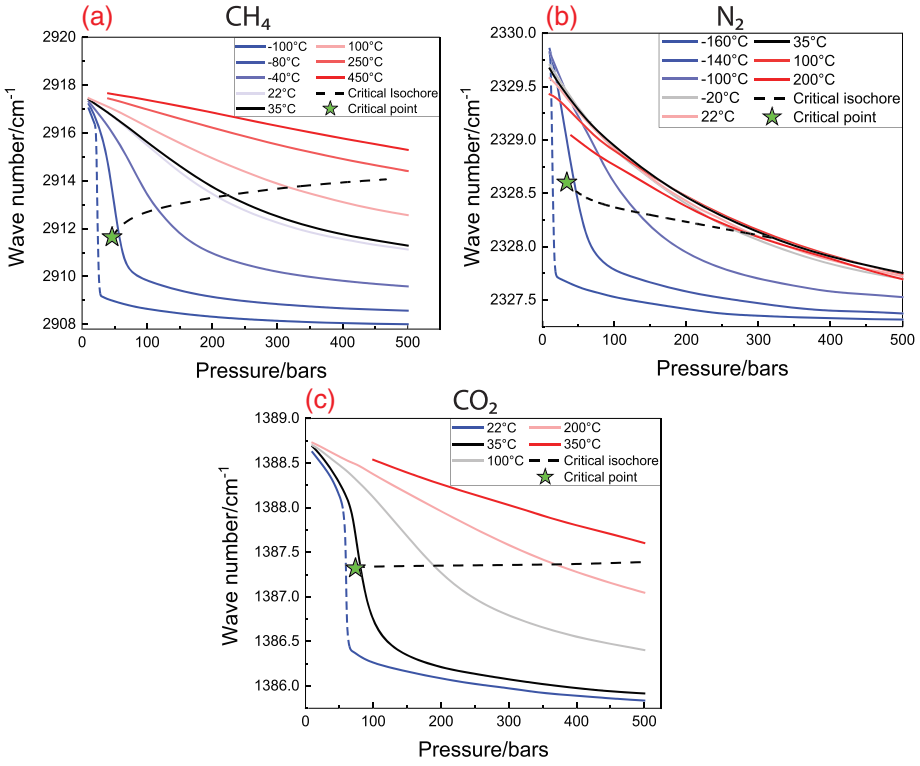

FIGURE 1 Plots of the peak position of (a) CH_4, (b) N_2, (c) and CO_2 versus pressure over the temperature ranges studied. The green star represents the critical point for each species, whereas the black dashed line represents the critical isochore. The dashed portion of the lowest temperature isotherm for each species represents the discontinuity in peak position as the liquid–vapor curve is intersected by the isotherm [Colour figure can be viewed at wileyonlinelibrary.com]

of the critical isochore correspond to fluids with densities greater than the critical density and are more liquid-like, whereas conditions to the right of the critical isochore correspond to fluids with densities less than the critical density and are more vapor-like.

The critical point of N_2 (Figure 1b) is located at −147°C and 34 bars, and the −160°C isotherm intersects the L–V curve at ~12 bars, as shown by the discontinuity along the −160°C isotherm represented by the dashed portion of the isotherm. As with CH_4, the peak position of N_2 decreases at constant temperature with increasing pressure over the entire temperature range studied. However, unlike CH_4, there is a reversal in the direction of the peak shift at pressures above 50 bars and temperatures between 0°C and 50°C (depending on pressure). At pressures above the transition pressure, the peak position increases with increasing temperature at constant pressure rather than decreasing with increasing temperature at constant pressure. At temperatures <100°C and a pressure of ~50 bars, the projections of the isotherms in pressure-peak position space intersect. Below ~50 bars, the temperature at which the peak position begins to decrease along an isobar is much lower than the temperature at which the peak position begins to decrease for pressures above 50 bars. For example, at 300 bars, the peak position decreases with increasing temperature above 35°C, whereas at 20 bars, the peak position decreases with increasing temperature above −120°C. A possible explanation for this reversal in peak shift is provided below.

The critical point of CO_2 is located at 31°C and 74 bars, and the 22°C isotherm intersects the L–V curve at ~60 bars (Figure 1c), as evidenced by the discontinuity along this isotherm represented by the dashed portion of the isotherm. Similar to both CH_4 and N_2, the peak position of CO_2 decreases with increasing pressure along an isotherm over the *PT* range studied. Also, similar to CH_4, at a constant pressure, the peak position increases with increasing temperature over the pressure range studied.

3.2 | Isothermal peak shift with changing density

The relationship between density and peak position for each gas along select isotherms is shown in Figure 2. Densities were calculated using the National Institute of Standards and Technology Reference Fluid Thermodynamic and Transport Properties Version 10.0 program[49] and the Setzman and Wagner,[50] Span et al.,[51] and Span and Wagner[52] equations of state for CH_4, N_2, and CO_2, respectively. All three gases show a decrease in peak position with increasing density. Both CH_4 (Figure 2a) and CO_2 (Figure 2c) show an increase in peak position with increasing temperature at a constant density, with the exception of the temperature range 350–450°C for CH_4

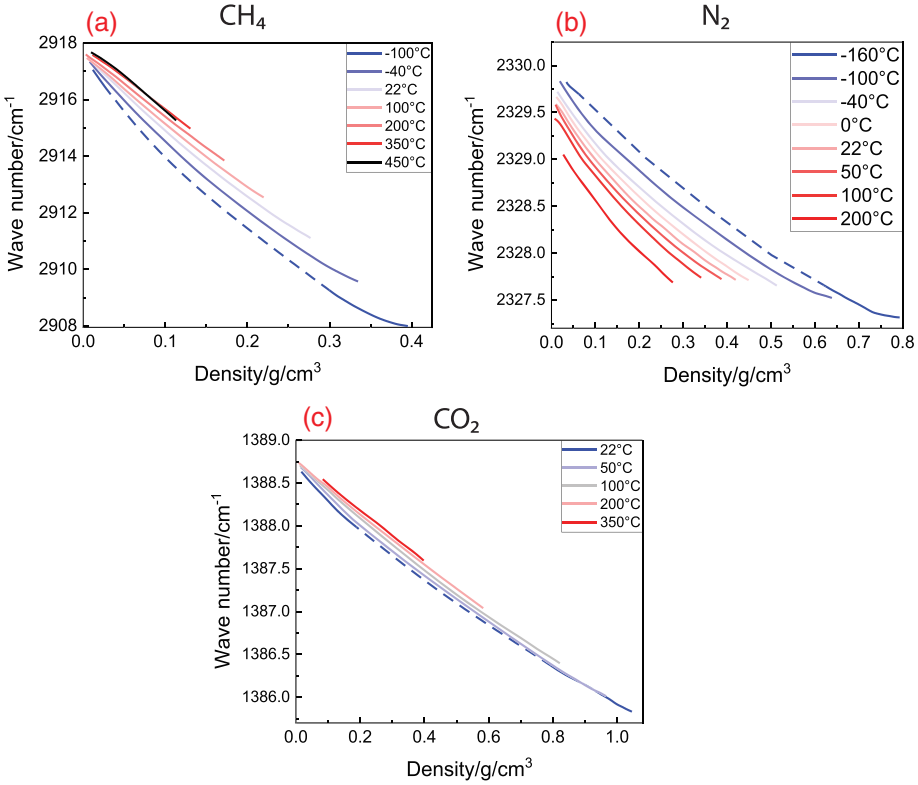

FIGURE 2 Plots of the peak position of (a) CH_4, (b) N_2, (c) and CO_2 versus density over the temperature ranges studied. Densities were calculated using the National Institute of Standards and Technology Reference Fluid Thermodynamic and Transport Properties Version 10.0 program[49] and the Setzman and Wagner,[50] Span et al,[51] and Span and Wagner,[52] equations of state for CH_4, N_2, and CO_2, respectively. The dashed portion of the lowest temperature isotherm for each species represents the discontinuity in peak position as the liquid–vapor curve is intersected by the isotherm [Colour figure can be viewed at wileyonlinelibrary.com]

(discussed further below). N_2 (Figure 2b) shows a decrease in peak position with increasing temperature at constant density over the studied region. The density-peak position relationship for CH_4 shown in Figure 2a is similar to that reported by Lin et al.[17] and Shang et al.[34] The density-peak position relationship for CO_2 shown in Figure 2c is similar to that reported by Wang et al.[47]

3.3 | Isobaric Peak shift with changing temperature

Figure 3 shows the relationship between temperature and peak position (solid lines) and temperature and density (dashed lines) at 40–500 bars for each species. CH_4 (Figure 3a) and CO_2 (Figure 3c) both show an initial sharp increase in peak position with increasing temperature at a constant pressure above the critical temperature, followed by a more gradual increase in peak position at higher temperatures. Note that a discontinuity occurs along the 40-bar isobar for CH_4 as the L–V curve is crossed. N_2 (Figure 3b) also shows an initial sharp increase in peak position with increasing temperature, followed by a more gradual increase at higher temperatures; however, at temperatures above ~0°C to 50°C, depending on pressure, the peak position decreases with increasing temperature. The variations in peak position with temperature broadly mirror the changes in density with temperature along the same isobar. For example, at 40 and 100 bars, both the peak position and the density show significant variation as the temperature is increased from the lowest values plotted for all three gases and a much less pronounced change in both peak position and density at higher temperature.

3.4 | Compressibility factor and peak position in PT space

Pressure–volume–temperature (*PVT*) data for gases may be examined using the unitless compressibility factor, *Z*, described by the following:

$$Z = \frac{PV_m}{RT}, \tag{2}$$

where V_m is molar volume and *R* is the gas constant. For compressibility factors used in this study, V_m is determined using the calculated densities described above. By definition, $Z = 1$ for an ideal gas. A gas with a compressibility factor less than unity has a density greater than the density of an ideal gas at the same *PT* conditions, whereas a gas with a compressibility factor greater than unity has a density that is less than the density of an ideal gas at the same *PT* conditions. Additionally, values of *Z* less than unity indicate an environment dominated by attractive interactions between molecules, whereas values of *Z* greater than unity indicate an environment dominated by repulsive interactions between molecules.

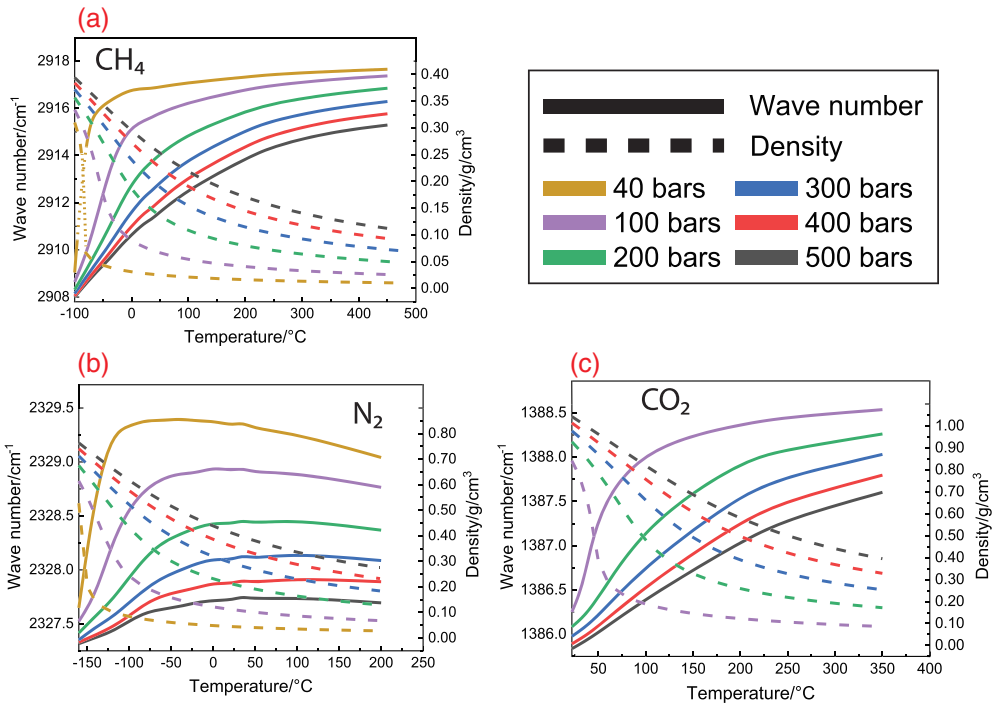

FIGURE 3 Plot of the peak position (solid lines) and the density (dashed lines) of (a) CH_4, (b) N_2, (c) and CO_2 versus temperature for several isobars. The dotted portion of the 40-bar isobars in (a) indicate the discontinuity in peak position and density as the liquid–vapor curve was intersected by the isobars between −100°C and −80°C. Densities were calculated using the National Institute of Standards and Technology Reference Fluid Thermodynamic and Transport Properties Version 10.0 program[49] and the Setzman and Wagner,[50] Span et al,[51] and Span and Wagner[52] equations of state for CH_4, N_2, and CO_2, respectively [Colour figure can be viewed at wileyonlinelibrary.com]

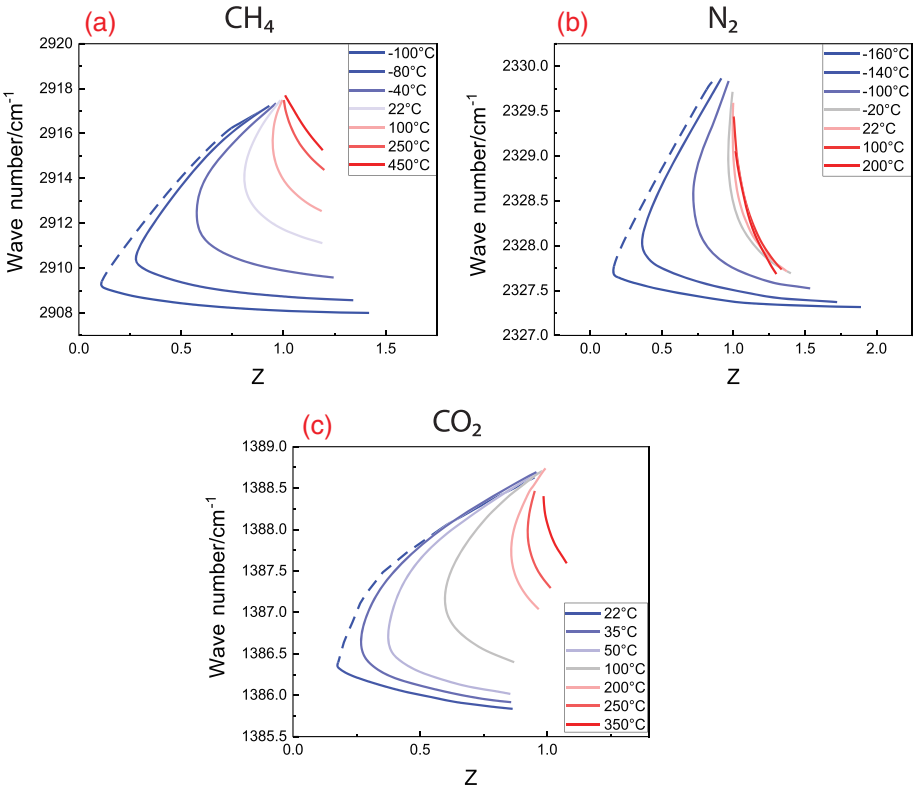

FIGURE 4 Plots of the peak position of (a) CH_4, (b) N_2, (c) and CO_2 versus compressibility factor (Z) over the temperature ranges studied. The dashed portion of the lowest temperature isotherm for each species represents the discontinuity in peak position as the liquid–vapor curve is intersected by the isotherm [Colour figure can be viewed at wileyonlinelibrary.com]

The relationship between the compressibility factor and peak position for each species studied here is shown in Figure 4. At higher temperatures, the range in compressibility factors is smaller and remains close to unity, as is expected because at higher temperatures the fluid is more gas-like (lower density), and lower density fluids behave more ideally. All three species show an increasing range in the compressibility factor with decreasing temperature over the pressure range studied. This reflects the fact that the fluids are becoming less ideal (more liquid-like) at lower temperatures.

The variation in peak position in *PT* space is shown in Figure 5. The solid black lines on Figure 5 represent "isofreqs" or lines of constant peak position (constant wave number). Isochores (lines of constant density) are also plotted in Figure 5. The isofreqs for CH_4 (Figure 5a) and CO_2 (Figure 5c) are roughly parallel to the isochores, especially for CO_2. For N_2 (Figure 5b), the isofreqs and isochores remain roughly parallel at lower temperatures, but the isofreqs begin to curve, and the slope changes from positive to negative with increasing temperature.

3.5 | Densimeters and barometers

Many studies have examined the relationship between Raman peak position and density or pressure and have developed algorithms and equations describing the relationship. The goal of many of these studies was to develop densimeters and barometers that can be used to determine the pressures (or densities) of fluids contained in natural fluid inclusions from various geologic environments on the basis of Raman analysis[16,18,20,34,45–47]. As such, we have fit our data, shown in Figures 1 and 2 and included in Appendix A, to develop equations describing the relationship between pressure, temperature, and density for the gases studied here. The main goal of the present study was not to develop densimeters or barometers but rather to understand the relationship between Raman peak positions as a function of pressure, temperature, and density for use in a follow-up study to examine the behavior of these gases in mixtures. Nonetheless, the equations developed and presented below may be used to determine the pressure (or density) of single component fluids trapped in fluid inclusions (and in other applications) as a function of peak position and temperature.

In developing the relationship between peak position, pressure, density, and temperature in this study, we employed the reduced temperature (T_R) of each gas.

$$T_R = \frac{T}{T_C}, \tag{3}$$

where T is temperature in Kelvin and T_c is the critical temperature of the gas in Kelvin. Using the reduced temperature, T_R, rather than the actual temperature

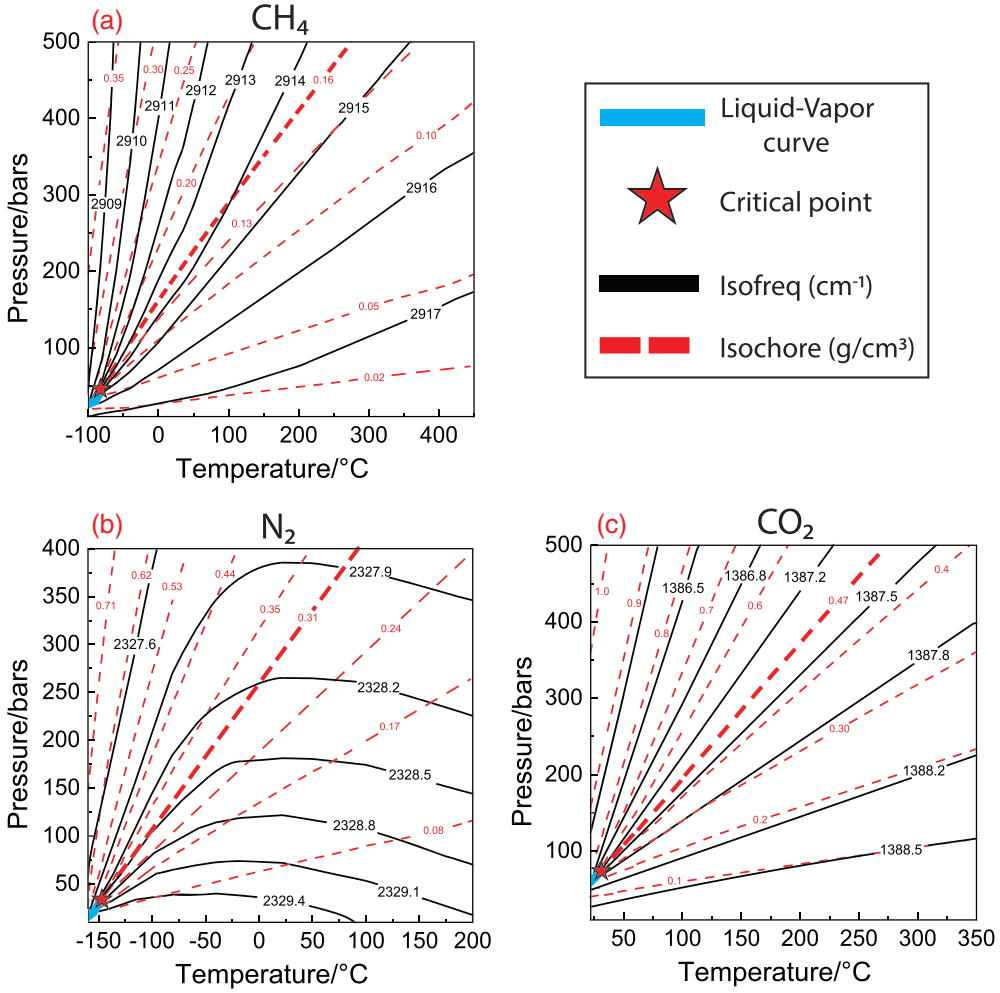

FIGURE 5 Plot of pressure versus temperature for (a) CH_4, (b) N_2, and (c) CO_2. Solid black lines are lines of constant peak position (isofreqs). Red dashed lines are lines of constant density (isochores). The bolded red dashed line in each figure represents the critical isochore. The star symbol represents the critical point of each system, and the solid blue line represents the liquid–vapor curve [Colour figure can be viewed at wileyonlinelibrary.com]

offers no advantages when evaluating data for the pure gases, but it does offer significant advantages when considering gas mixtures at temperatures at which the gas mixture does not undergo a phase change (i.e., consist of liquid and vapor or two immiscible fluid phases) whereas one of the components of the mixture would undergo a phase change at those same PT conditions. For example, pure CO_2 undergoes a phase transition at 22°C when the L–V curve is intersected (see Figure 1c). However, for a gas mixture containing CO_2, CH_4, and N_2 with a critical point sufficiently less than 22°C such that the maxcondentherm of the dew point curve is at a temperature lower than 22°C, a phase change will not occur as pressure is changed at 22°C. Thus, the peak positions and Fermi diad splitting measured for CO_2 in the gas mixture change continuously as pressure is increased at 22°C whereas a discontinuity occurs in the peak positions and Fermi diad splitting in pure CO_2 at the same conditions when the L–V curve is crossed. Using the reduced temperature for this example mixture would circumvent the phase transition and the accompanying discontinuity in pressure-peak position space experienced by pure CO_2. As such, the reduced temperature, T_R, is used in the densimeters and barometers presented here to facilitate incorporation of these algorithms into those being developed for gas mixtures.

The densimeter for CH_4 is valid from 10 to 500 bars and −100°C to 450°C and is given by

$$\rho_{CH_4} = \sum_{i=0}^{2}\sum_{j=2}^{2} A_{i,j}(T_R)^i(\nu - 2{,}917)^j, \qquad (4)$$

where ρ is density in grams per cubic centimeter and ν is the Raman peak position in per centimeter. The fitting coefficients and associated errors are given in Table 1. Equation (4) has an R^2 of 0.998 and a standard error of ±0.003 g/cm^3. The barometer for CH_4, which is valid from 10 to 500 bars and −80°C to 350°C, is given by

$$P_{CH_4} = \frac{\sum_{i=0}^{2}\sum_{j=0}^{2} A_{i,j}(\nu - 2917)^i(T_R)^j}{1 + \sum_{k=0}^{2}\sum_{l=0}^{2} B_{k,l}(\nu - 2917)^k(T_R)^l}, \qquad (5)$$

TABLE 1 Fitting coefficients for the CH_4 densimeter (Equation (4))

$A_{i,j}$	Value	Error (±)
0,0	−0.01317	0.00435
1,0	0.03021	0.00389
2,0	−0.0046	7.78×10^{-4}
0,1	−0.01897	0.00140
0,2	0.00161	1.03×10^{-4}
1,1	−0.00867	5.60×10^{-4}

TABLE 2 Fitting coefficients for the CH_4 barometer (Equation (5))

$A_{i,j}$	Value	Error (±)
0,0	41.24	9.04
1,0	77.11	2.29
0,1	−47.09	9.04
0,2	25.00	1.96
1,1	−82.47	2.19
$B_{k,l}$	Value	Error (±)
1,0	−0.31255	0.00539
2,0	−0.03746	7.04×10^{-4}
0,1	−0.1796	0.0272
0,2	0.07054	0.00607
1,1	0.08383	0.00265

where P is in bars. The fitting coefficients and associated errors are given in Table 2. Equation (5) has an R^2 of 0.997 and a standard error of ±9.8 bars. Because the data from Lin et al.[17] at 22°C were used to develop the CH_4 barometer and densimeter, Equations (4) and (5) agree with Lin et al.[17] within analytical error.

The densimeter for N_2 is valid from 10 to 500 bars and −160°C to 200°C and is given by the following:

$$\rho_{N_2} = \sum_{i=0}^{2}\sum_{j=2}^{2} A_{i,j}(T_R)^i \left\{\ln\left[\left(\frac{\nu \cdot 1000}{2330}\right) - 998\right]\right\}^j. \quad (6)$$

The ν term in Equation (6) is presented in this manner to accentuate the small changes in the Raman peak position of N_2 with changing pressure over the PT range studied. The fitting coefficients and associated errors are given in Table 3. Equation (6) has an R^2 of 0.999 and a standard error of ±0.008 g/cm^3. The barometer for N_2 is valid from 10 to 500 bars and −140°C to 200°C and is given by the following:

TABLE 3 Fitting coefficients for the N_2 densimeter (Equation (6))

$A_{i,j}$	Value	Error (±)
0,0	2.0719	0.0136
1,0	−0.25827	0.00494
2,0	0.00638	8.39×10^{-4}
0,1	−1.6203	0.0221
0,2	0.30296	0.00779
1,1	0.10800	0.00254

$$P_{N_2} = \frac{\sum_{i=0}^{2}\sum_{j=0}^{2} A_{i,j}\left\{\ln\left[\left(\frac{\nu \cdot 1000}{2330}\right) - 998\right]\right\}^i (T_R)^j}{1 + \sum_{k=0}^{2}\sum_{l=0}^{2} B_{k,l}\left\{\ln\left[\left(\frac{\nu \cdot 1000}{2330}\right) - 998\right]\right\}^k (T_R)^l}. \quad (7)$$

The fitting coefficients and associated errors are given in Table 4. Equation (7) has an R^2 of 0.996 and a standard error of ±12.4 bars.

For CO_2, the splitting of the Fermi diad is more commonly used than a single peak position to correlate Raman spectral features with pressure or density because the distance between the two peaks that make up the Fermi diad remains relatively constant and independent of instrument drift. As such, the densimeter and barometer for CO_2 were developed using the Fermi diad splitting. The densimeter for CO_2 is valid from 10 to 500 bars and 22°C to 350°C and is given by the following:

$$\rho_{CO_2} = \sum_{i=0}^{1}\sum_{j=2}^{2} A_{i,j}(T_R)^i(\Delta - 100)^j, \quad (8)$$

where Δ is the Fermi diad splitting in per centimeter. The fitting coefficients and associated errors are given in Table 5. Equation (8) has an R^2 of 0.999 and a standard

TABLE 4 Fitting coefficients for the N_2 barometer (Equation (7))

$A_{i,j}$	Value	Error (±)
0,0	−5.930	0.404
1,0	6.042	0.871
0,1	8.749	0.406
0,2	−0.9672	0.0769
1,1	−8.429	0.760
$B_{k,l}$	Value	Error (±)
1,0	6.037	0.106
2,0	3.989	0.363
0,2	0.1307	0.0198
1,1	−1.5546	0.0380

TABLE 5 Fitting coefficients for the CO_2 densimeter (Equation (8))

$A_{i,j}$	Value	Error (±)
0,0	−1.1429	0.0940
1,0	−0.3144	0.0436
0,1	0.4461	0.0425
0,2	−0.02296	0.00392
1,1	0.1529	0.0144

TABLE 6 Fitting coefficients for the CO_2 barometer (Equation (9))

$A_{i,j}$	Value	Error (±)
0,0	3090	1250
1,0	−1019	420
0,1	−3420	1380
0,2	161.7	70.3
1,1	1108	456
$B_{k,l}$	**Value**	**Error (±)**
1,0	2.685	0.941
2,0	−0.430	0.144
0,1	−3.683	0.882
0,2	0.909	0.217

error of ±0.006 g/cm^3. The barometer for CO_2 is valid from 10 to 500 bars and 35°C to 350°C and is given by the following:

$$P_{CO_2} = \frac{\sum_{i=0}^{2}\sum_{j=0}^{2} A_{i,j}(\Delta - 100)^i (T_R)^j}{1 + \sum_{k=0}^{2}\sum_{l=0}^{2} B_{k,l}(\Delta - 100)^k (T_R)^l}. \quad (9)$$

The fitting coefficients and associated errors are given in Table 6. Equation (9) has an R^2 of 0.995 and a standard error of ±6.2 bars. Because the data from Fall et al.[18] at 22°C were used to develop the CO_2 densimeter, Equation (8) agrees with Fall et al.[18] within analytical error.

4 | DISCUSSION

4.1 | Peak position and criticality

The variation in peak position with PT is related to the relative density (volume) changes that occur during a change in *PT* conditions. This is exemplified in Figure 3, as the isobars in temperature-peak position and temperature–density space show complementary trends. The largest changes in both density and peak position with temperature occur at the lowest temperatures shown, that is, near the critical point, and the relative change in peak position and density as a function of temperature is muted at higher temperatures. However, as noted above, the isofreqs for N_2 reach a maximum pressure at some temperature and then decrease in pressure as temperature increases further. This reversal in the peak position trend with increasing pressure may be related to changes in the attractive and repulsive forces and is discussed further below. The largest relative density (volume) changes coincide with the largest relative peak position changes for each gas and occur in the vicinity of the critical point for that gas. This is expected because thermodynamic properties of fluids, such as heat capacity, isobaric thermal expansivity, and isothermal compressibility,[53] show large (infinite) changes with changing P or T near the critical point.[54]

The shape of the isotherms of each gas and magnitude of the peak shift along an isotherm in pressure-peak position space shown in Figure 1 is systematically related to the proximity of the isotherm to the critical point. Reduced temperature (Equation (3)) serves as a convenient proxy for nearness to the critical temperature, with a reduced temperature of unity ($T_r = 1$) corresponding to a temperature equal to the critical temperature. The low temperature isotherms show a larger shift in peak position with increasing pressure over the *PT* range studied, compared with the higher temperature isotherms, and have a more sigmoidal shape compared with the more linear high temperature isotherms (see Figure 1). Note that the isotherms in Figure 1 that are below the critical temperature are discontinuous where the isotherm crosses the L–V curve and are thus not considered sigmoidal. The degree to which the isotherm is sigmoidal in pressure-peak position space depends on the reduced temperature of the gas, as small changes in pressure in the vicinity of the critical point result in large relative changes in density (volume). This can be seen clearly using the 35°C isotherms (solid black lines in Figure 1a, b,c) for CH_4, N_2, and CO_2. At 35°C, the T_R for CO_2, CH_4, and N_2 is 1.1, 1.6, and 2.4, respectively. The 35°C isotherm for CO_2 shows the most pronounced relative peak shift of the three gases at 35°C because it is closest to its critical temperature at 35°C and experiences the largest relative density (volume) change along the 35°C isotherm with increasing pressure. In contrast, N_2 shows the least pronounced relative peak shift of the three gases, partly due to the fact that at 35°C, the gas is well above the critical temperature of N_2 (−147°C) and the relative density (volume) change with pressure is smaller than that of CO_2 at 35°C. CH_4 shows a behavior that is intermediate

between that shown for CO_2 and N_2, consistent with the fact that the critical temperature of CH_4 (−83°C) is between those for CO_2 (31°C) and N_2 (−147°C).

4.2 | Interpretation of Raman spectra using intermolecular attraction and repulsion

The variation in Raman peak position with *PT* reflects interactions between molecules. As noted above, dominance of attractive forces leads to a shift in the Raman peak position to lower wave numbers whereas dominance of repulsive forces leads to a shift in the Raman peak position to higher wave numbers.[21,38,39] The reason for this is that dominance of repulsive forces contracts the bond length slightly whereas dominance of attractive forces expands the bond length slightly.[55] Contraction of the bond strengthens the bond, requiring more energy to cause a vibration, whereas expansion of the bond weakens the bond, requiring less energy to cause a vibration.[17] The strength of the repulsive and attractive forces between molecules is dependent on the distance between molecules, with repulsive forces between molecules being most intense when the molecules are in close proximity to one another and attractive forces being experienced between molecules at longer intermolecular distances.[40]

4.2.1 | Isothermal inflection pressure

Pressure and temperature have opposing effects on the volume of the gas and the distance between molecules: increasing pressure decreases volume and increasing temperature increases volume. Attractive forces between molecules dominate at greater intermolecular distances than repulsive forces, so at low pressures and high temperatures where the molecules are spaced sufficiently far apart such that the repulsive forces between molecules are insignificant, a small decrease in volume is expected to yield an overall negative shift in Raman peak position. This overall negative shift in peak position can be seen in Figures 1 and 2. As volume decreases further and repulsive forces between molecules increase, attractive and repulsive forces produce competing effects on the wave number shift. Additionally, the relative increase in the magnitude of the attractive forces decreases as the molecules are forced closer together, whereas the magnitude of the repulsive forces increases.[40] This implies that at a constant temperature and sufficiently high pressure (higher than the pressure range studied here for N_2, CO_2, and CH_4), the repulsive forces become dominant, and the peak position increases with increasing pressure along the isotherm. This phenomenon, in which the isothermal pressure dependence of peak position shows an inflection with increasing pressure, has been observed for N_2, CH_4, and H_2[15,21]. The pressure of this inflection point at 22°C is ~1,000 bars for CH_4 and ~1,500 bars for N_2[15]. Note that these pressure inflection points are likely temperature dependent.

4.2.2 | Isobaric inflection temperature

If the peak position increases along an isobar as temperature increases (see Figures 1 and 3), repulsive forces between molecules are dominant. This behavior is potentially related to the increasing frequency of collisions brought about by increasing the kinetic energy of the molecules. However, increasing temperature at constant pressure will also increase the volume and thus intermolecular distance, which will weaken the effect of the repulsive forces whereas the attractive forces, which are experienced between molecules at larger intermolecular distance than repulsive forces, will not change much until the intermolecular distances are sufficiently large that the molecules do not interact at all and behave like an ideal gas. This implies that at a constant pressure and relatively high temperature, the repulsive forces would be sufficiently weakened such that attractive forces dominate and the peak position will shift to lower wave numbers. Thus, in a manner similar to the isothermal pressure dependence of peak position, the isobaric temperature dependence of peak position also shows an inflection and change in trend with increasing temperature. This can be seen for N_2 in Figures 1b and 3b, where the inflection occurs between 0°C and 50°C (depending on the pressure) above ~50 bars and at much lower temperatures below ~50 bars. A potential explanation for the inflection occurring at much lower temperatures at pressures less than ~50 bars is that the molecules are spaced sufficiently far apart that only a small temperature increase is needed to reduce the repulsive interactions beyond the inflection point, resulting in the much lower inflection temperatures found for N_2 at pressures less than ~50 bars. Although the inflection temperature was not reached for CH_4 and CO_2, the decreasing difference in peak position between isotherms separated by the same temperature increment in Figure 1a,c indicates that the inflection temperature is being approached, with CH_4 appearing to be closer to the inflection temperature than CO_2 at 350°C. This relative order of inflection temperatures in pressure-wave number space is further supported by the 450°C isotherm shown in Figure 2a (black line) for CH_4. The peak positions of CH_4 at densities above

~0.06 g/cm^3 at 450°C are at lower wave numbers than the peak position of CH_4 at densities above ~0.06 g/cm^3 at 350°C. As can be seen from Figure 2b relative to Figure 1b, the inflection temperature for N_2 is located at a lower temperature in density-wave number space (isochoric inflection temperature) than pressure-wave number space (isobaric inflection temperature). Because CH_4 has reached the isochoric inflection temperature over the *PT* range studied and CO_2 has not, it is likely that CH_4 will also reach the isobaric inflection temperature before CO_2. The order in which the species reach this inflection temperature can be related to the Boyle temperature of the molecules, which is the temperature at which the attractive and repulsive forces are equivalent and of opposite sign such that they cancel out. The Boyle temperature defined at 0 pressure for N_2, CH_4, and CO_2 is ~50°C, ~240°C, and ~450°C, respectively.[56] The inflection temperatures do not occur exactly at the Boyle temperatures, however, from the Boyle temperatures, it would be expected that N_2, which has the lowest Boyle temperature, would have an inflection temperature lower than that of CH_4, which, in turn, would be located at a lower temperature than CO_2. The results shown in Figure 1 are in good agreement with this interpretation.

4.3 | Relationship between isochores and isofreqs for N_2, CH_4, and CO_2

Initially, starting from low pressures and temperatures, the effect of increasing *PT* on the shift in peak position reflects competing effects of intermolecular interactions, similar to the manner in which increasing temperature and pressure have competing effects on the density. However, depending on the *PT* conditions at which the inflection points are reached, the effects of increasing temperature and pressure may no longer act against each other with regard to the shift in the peak position but instead may act in the same direction, leading to the curvature of the isofreqs in Figure 5. Note that the isofreqs in Figure 5c are nearly linear due to the fact that CO_2 is well below both the isobaric inflection temperature and the isothermal inflection pressure in the *PT* range studied. Using the 0.35 g/cm^3 isochore in Figure 5b (N_2) as an example, as temperature is increased along the isochore, the pressure must also increase to maintain a constant volume (density) because of the opposing effects of compressibility and thermal expansivity. The isochore by definition represents the locus of *P* and *T* along which these opposing effects are equal and thus cancel out to maintain constant density. The same *PT* relationship can be invoked for the 2,328.2 cm^{-1} isofreq in Figure 5b over the *PT* range up to approximately −80°C and ~180 bars, where the isofreq remains roughly parallel to the 0.35 g/cm^3 isochore. As temperature is increased along the isofreq, pressure must also increase to maintain a constant peak position (wave number) because increasing temperature alone at conditions below the isobaric temperature inflection point results in an increase in the peak position (Figure 3). Below the isothermal pressure inflection point, increasing pressure leads to a decrease in the peak position (Figure 1b). Thus, similar to the case of density along the isochore, along the isofreq (below the inflection point of one of the variables), increasing *P* and *T* have equal and opposite effects on the peak position and cancel each other. However, unlike the isochores, the isofreqs must curve as the inflection point of one variable, either *P* or *T*, is reached such that the two effects become *complementary* instead of opposing. This results in the change in slope of the 2,328.2 cm^{-1} isofreq in Figure 5b from positive to negative at ~22°C, at which point the isofreq reaches the *T* inflection. Thus, to maintain the constant peak position as *T* increases above ~22°C, pressure must now *decrease* instead of increase.

5 | SUMMARY

Raman spectra were collected for the symmetric stretching peak of N_2, CO_2, and CH_4 from 10 to 500 bars and from temperatures slightly below the L–V curve to elevated temperatures. Volumetric changes and the resulting changes in intermolecular forces affect the magnitude and direction of Raman peak shifts of N_2, CH_4, and CO_2 over the *PT* range studied. The competing effects of attraction and repulsion between molecules are revealed through changes in peak position. Moreover, the volumetric changes and intermolecular interactions associated with these volumetric changes are correlated to proximity of the analytical conditions to the critical temperature that in turn gives rise to a systematic relationship between Raman peak positions of these fluids and criticality. The information gathered on the pure gases can be expanded in future work to gas mixtures containing N_2, CO_2, and CH_4.

ACKNOWLEDGEMENTS

The authors thank Charles Farley for assistance in the laboratory and Yury Klyukin and Lowell Moore for many helpful conversations on intermolecular forces and Kyle Ashley for helpful discussions of pressure and temperature dependence of Raman peaks and drift during Raman measurements. This material is based in part on work supported by the National Science Foundation under Grants EAR-1624589 and OCE-1459433 to R. J. B. H.

M. L was supported by the PFF fellowship at the University of Missouri. M. S-M was supported by a Discovery Grant from NSERC. G. S. was supported by the KoUP Cooperation Funding program of the University of Potsdam. R. C. B was supported by the Energy Resources Program of the U.S. Geological Survey. Use of trade, product, or firm names is for descriptive purposes only and does not imply endorsement by the U.S. government.

REFERENCES

[1] H. E. C. Swanenberg, *Geologica Ultraiectina* **1980**, *25*, 1.
[2] J. Touret, in *Short course in fluid inclusions: Application to petrology*, (Eds: L. S. Hollister, M. L. Crawford), Mineral association of Canada, Markham **1981** 182.
[3] R. Kreulen, R. D. Schuiling, *Geochim. Cosmochim. Acta* **1982**, *46*, 193.
[4] A. M. Van den Kerkhof, *Ph. D. thesis*, Univ. Amsterdam, **1988**.
[5] C. J. S. DeAlvarenga, M. Cathelineau, J. Dubessy, *Mineral. Mag.* **1990**, *54*, 245.
[6] P. D. Jenden, I. R. Kaplan, R. Poreda, H. Craig, *Geochim. Cosmochim. Acta* **1988**, *52*, 851.
[7] L. Palcsu, I. Vető, I. Futó, G. Vodila, L. Papp, Z. Major, *Marine Petrol. Geol.* **2014**, *54*, 216.
[8] E. L. Klein, C. Harris, C. Renac, A. Giret, C. A. V. Moura, K. Fuzikawa, *Miner. Depositia* **2006**, *41*, 160.
[9] E. Chicharro, M. Boiron, J. A. López-García, D. N. Bardfod, C. Villaseca, *Ore Geol. Rev.* **2016**, *72*, 896.
[10] H. B. Niemann, S. K. Atreya, S. J. Bauer, G. R. Carignan, J. E. Demick, R. L. Frost, D. Gautier, J. A. Haberman, D. N. Harpold, D. M. Hunten, G. Israel, J. I. Lunine, W. T. Kasprzak, T. C. Owen, M. Paulkovich, F. Raulin, E. Raaen, S. H. Way, *Nature* **2005**, *438*, 779.
[11] H. B. Niemann, S. K. Atreya, J. E. Demick, D. Gautier, J. A. Haberman, D. N. Harpold, W. T. Kasprzak, J. I. Lunine, T. C. Owen, F. Raulin, *J. Geophys. Res. E Planets* **2010**, *115*, 1.
[12] X. Zang, D. Liang, *J. Chem. Eng. Data* **2018**, *63*, 197.
[13] D. V. Petrov, *Spectrochim. Acta A* **2018**, *191*, 576.
[14] D. A. Long, *The Raman effect: A unified treatment of the theory of Raman scattering by molecules*, John Wiley & Sons, Chichester **2002**.
[15] D. Fabre, B. Oksengorn, *Appl. Spectrosc.* **1992**, *46*, 468.
[16] F. Lin, R. J. Bodnar, S. P. Becker, *Geochim. Cosmochim. Acta* **2007**, *71*, 3746.
[17] F. Lin, A. K. Sum, R. J. Bodnar, *J. Raman. Spectrosc.* **2007**, *38*, 1510.
[18] A. Fall, B. Tattitch, R. J. Bodnar, *Geochim. Cosmochim. Acta* **2011**, *75*, 951.
[19] H. M. Lamadrid, M. Steele-MacInnis, R. J. Bodnar, *J. Raman. Spectrosc.* **2018**, *49*, 581.
[20] H. M. Lamadrid, L. R. Moore, D. Moncada, J. D. Rimstidt, R. C. Burruss, R. J. Bodnar, *Chem. Geol.* **2017**, *450*, 210.
[21] A. D. May, V. Degen, J. C. Stryland, H. L. Welsh, *Can. J. Phys.* **1961**, *39*, 1769.
[22] D. Fabre, R. Couty, *Comptes Rendus L Acad Des Sci Ser II* **1986**, *303*, 1305.
[23] R. Kroon, M. Baggen, A. Lagendijk, *J. Chem. Phys.* **1989**, *97*, 74.
[24] B. Lavorel, B. Oksengorn, D. Fabre, R. Saint-Loup, H. Berger, *Mol. Phys.* **1992**, *75*, 397.
[25] M. J. Clouter, H. Kiefte, *J. Chem. Phys.* **1977**, *66*, 1736.
[26] M. J. Clouter, H. Kiefte, R. K. Jain, *J. Chem. Phys.* **1980**, *73*, 673.
[27] B. Oksengorn, D. Fabre, B. Lavorel, R. Saint-Loup, H. Berger, *J. Chem. Phys.* **1991**, *94*, 1774.
[28] R. D. Etters, J. Belak, R. LeSar, *Phys. Rev. B* **1986**, *34*, 4221.
[29] T. Dreier, G. Schiff, A. A. Suvernev, *J. Chem. Phys.* **1994**, *100*, 6275.
[30] G. S. Devendorf, D. Ben-Amotz, *J. Phys. Chem.* **1993**, *97*, 2307.
[31] J. C. Seitz, J. D. Pasteris, I.-M. Chou, *Amer. J. Sci.* **1993**, *293*, 297.
[32] I.-M. Chou, J. D. Pasteris, J. C. Seitz, *Geochim. Cosmochim. Acta* **1990**, *54*, 535.
[33] V. Thieu, S. Subramanian, S. O. Colgate, E. D. Sloan Jr., *Ann. N. Y. Acad. Sci.* **2000**, *912*, 983.
[34] L. Shang, I.-M. Chou, R. C. Burruss, R. Hu, X. Bi, *J. Raman Spectrosc.* **2014**, *45*, 696.
[35] W. Lu, I.-M. Chou, R. C. Burruss, Y. Song, *Geochim. Cosmochim. Acta* **2007**, *71*, 3969.
[36] J. C. Seitz, J. D. Pasteris, I.-M. Chou, *Amer. J. Sci.* **1996**, *296*, 577.
[37] S. Brunsgaard Hansen, R. W. Berg, E. H. Stenby, *Appl. Spectrosc.* **2001**, *55*, 745.
[38] W. Schindler, J. Jonas, *J. Chem. Phys.* **1980**, *73*, 3547.
[39] W. Schindler, P. T. Sharko, J. Jonas, *J. Chem. Phys.* **1982**, *76*, 3493.
[40] K. S. Schweizer, D. Chandler, *J. Chem. Phys.* **1982**, *76*, 2296.
[41] B. Lavorel, R. Chaux, R. Saint-Loup, H. Berger, *Opt. Commun.* **1987**, *62*, 25.
[42] S. C. Schmidt, D. S. Moore, M. S. Shaw, *Phys. Rev. B* **1987**, *35*, 493.
[43] E. Fermi, *Z. Phys.* **1931**, *71*, 250.
[44] K. M. Rosso, R. J. Bodnar, *Geochim. Cosmochim. Acta* **1995**, *59*, 3961.
[45] Y. Kawakami, J. Yamamoto, H. Kagi, *Appl. Spectrosc.* **2003**, *57*, 1333.
[46] J. Yamamoto, H. Kagi, *Chem. Lett.* **2006**, *35*, 610.
[47] X. Wang, I.-M. Chou, W. Hu, R. C. Burruss, Q. Sun, Y. Song, *Geochim. Cosmochim. Acta* **2011**, *75*, 4080.
[48] I.-M. Chou, R. C. Burruss, W. Lu, in *Advancesin high-pressure technology for geophysics applications*, (Eds: J. Chen, Y. Wang, T. S. Duffy, G. Shen, L. F. Dobrzhinetskaya), Elsevier B. V., Amsterdam **2005** 475.
[49] E.W. Lemmon, I. H. Bell, M.L. Huber, M.O. McLinden, *NIST standard reference database 23: Reference fluid thermodynamic and transport properties-REFPROP, Version 10.0*, National Institute of Standards and Technology, Standard Reference Data Program, Gaithersburg, **2018**.
[50] U. Setzmann, W. Wagner, *J. Phys. Chem.* **1991**, *20*, 1061.
[51] R. Span, E. W. Lemmon, R. T. Jacobsen, W. Wagner, A. Yokozeki, *J. Phys. Chem.* **2000**, *29*, 1361.
[52] R. Span, W. Wagner, *J. Phys. Chem. Ref. Data Monogr.* **1996**, *25*, 1509.
[53] J. V. Sengers, J. M. H. Levelt Sengers, *Annu. Rev. Phys. Chem.* **1986**, *37*, 189.
[54] J. W. Johnson, D. Norton, *Am. J. Sci.* **1991**, *291*, 541.
[55] M. R. Zakin, D. R. Herschbach, *J. Chem. Phys.* **1986**, *85*, 2376.

[56] R. Estrada-Torres, G. A. Iglesias-Silva, M. Ramos-Estrada, K. R. Hall, *Fluid Phase Equilibria* **2007**, *258*, 148.

SUPPORTING INFORMATION

Additional supporting information may be found online in the Supporting Information section at the end of this article.

How to cite this article: Sublett Jr. DM, Sendula E, Lamadrid H, et al. Shift in the Raman symmetric stretching band of N_2, CO_2, and CH_4 as a function of temperature, pressure, and density. *J Raman Spectrosc*. 2020;51:555–568. https://doi.org/10.1002/jrs.5805